LETTERS
PUBLISHED ONLINE: 4 MARCH 2012 | DOI: 10.1038/NPHOTON.2012.34
nature photonics

Heralded quantum entanglement between two crystals

Imam Usmani, Christoph Clausen, Félix Bussières, Nicolas Sangouard, Mikael Afzelius* and Nicolas Gisin

Quantum networks must have the crucial ability to entangle quantum nodes[1]. A prominent example is the quantum repeater[2–4], which allows the distance barrier of direct transmission of single photons to be overcome, provided remote quantum memories can be entangled in a heralded fashion. Here, we report the observation of heralded entanglement between two ensembles of rare-earth ions doped into separate crystals. A heralded single photon is sent through a 50/50 beamsplitter, creating a single-photon entangled state delocalized between two spatial modes. The quantum state of each mode is subsequently mapped onto a crystal, leading to an entangled state consisting of a single collective excitation delocalized between two crystals. This entanglement is revealed by mapping it back to optical modes and by estimating the concurrence of the retrieved light state[5]. Our results highlight the potential of crystals doped with rare-earth ions for entangled quantum nodes and bring quantum networks based on solid-state resources one step closer.

Quantum entanglement challenges our intuition about physical reality. At the same time, it is an essential ingredient in quantum communication[6], quantum precision measurements[7] and quantum computing[8,9]. In quantum communication, photons are naturally used as carriers of entanglement using either free-space or optical-fibre transmission. However, even with ultralow-loss telecommunication optical fibre, the transmission probability decreases exponentially with distance, limiting the achievable communication distance to a few hundred kilometres[10]. A potential solution is to use quantum repeaters[2] based on linear optics and quantum memories[3,4] with which the entanglement distribution time scales polynomially with the transmission distance, provided entanglement between quantum memories in remote locations can be heralded. In this context, one can more generally consider prospective quantum networks[1] where nodes generate, process and store quantum information, while photons transport quantum states from site to site and distribute entanglement over the entire network. An essential step towards the implementation of such potential technologies is to create entanglement between two quantum memories in a heralded manner[3,4].

Experimental observation of heralded entanglement between two independent atomic systems for quantum networks has been achieved using cold gas ensembles involving either two distinct ensembles[5] or two spatial modes in the same ensemble[11–14]. Complete elementary links of a quantum repeater (based on heralded entanglement) have been implemented in cold gas systems[15,16] and with two trapped ions[17]. For the realization of scalable quantum repeaters, solid-state devices are technologically appealing[18]. In this context, important results have already been obtained by using crystals doped with rare-earth ions (REs) as quantum memories. These results have demonstrated light storage times greater than one second[19], a storage efficiency of 69% (ref. 20) and quantum storage of 64 independent optical modes in one crystal[21] (see also ref. 22). Recent achievements[23,24] include the storage, in a single RE-doped crystal, of photonic time-bin entanglement generated through spontaneous parametric downconversion (SPDC). Heralded entanglement between two RE-doped crystals using an SPDC source, a common resource in quantum optics, represents an important step towards the implementation of quantum repeater architectures based on solid-state devices[25].

Here, we present the observation of heralded quantum entanglement between two neodymium ensembles doped in two yttrium orthosilicate crystals (Nd^{3+}:Y_2SiO_5) separated by 1.3 cm (Fig. 1 and Methods). A nonlinear optical waveguide is pumped to produce photon pairs by means of SPDC. The resulting idler (1,338 nm) and signal (883 nm) photons are strongly filtered to match the working bandwidth of the crystals, yielding a coherence time of 7 ns. In the limit where the probability of creating a single pair is much smaller than one, the detection of an idler photon heralds the presence of a single signal photon. By sending the latter through a balanced beamsplitter, one heralds, neglecting optical losses, a single-photon entangled state[26] $1/\sqrt{2}(|1\rangle_A|0\rangle_B + |0\rangle_A|1\rangle_B)$ between the two spatial output modes A and B. In each of the modes a crystal acts as quantum memory, denoted M_A or M_B. Upon absorption of the single photon[27], the detection of an idler photon heralds the creation of a single collective excitation delocalized between the two crystals, written as $1/\sqrt{2}(|W\rangle_A|0\rangle_B + |0\rangle_A|W\rangle_B)$. Here, $|W\rangle_A$(or $|W\rangle_B$) is the Dicke-like state created by the absorption of a single photon in M_A (or M_B). To determine the presence of entanglement between the memories, we use a photon-echo technique based on an atomic frequency comb[27–31] that reconverts the collective excitation into optical modes A and B after a preprogrammed storage time of 33 ns (with a total efficiency of 15%). The resulting fields can then be probed using single-photon detectors to reveal heralded entanglement between the memories. As the entanglement cannot increase through local operations on the optical modes A and B, the entanglement of the retrieved light fields provides a lower bound for entanglement between the two memories.

The photonic state retrieved from the memories is described by a density matrix ρ, including loss and noise, expressed in the Fock state basis. To reveal entanglement in this basis, a tomographic approach based on single-photon detectors can be used[5,13,14]. Specifically, from the values of the heralded probabilities p_{mn} of detecting $m \in \{0,1\}$ photons in mode A and $n \in \{0,1\}$ in mode B, combined with the magnitude of the coherence between these modes, a lower bound on the concurrence C of the detected fields is obtained by

$$C \geq \max(0, V(p_{01} + p_{10}) - 2\sqrt{p_{00}p_{11}}) \quad (1)$$

Group of Applied Physics, University of Geneva, CH-1211 Geneva 4, Switzerland. *e-mail: mikael.afzelius@unige.ch

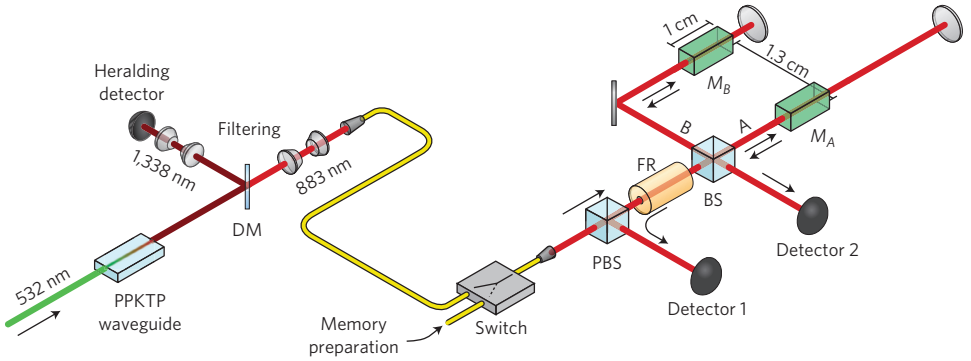

Figure 1 | Experimental set-up. Quantum memories M_A and M_B are implemented using neodymium ions doped into yttrium ortho-silicate crystals (Nd^{3+}:Y_2SiO_5) separated by 1.3 cm and cooled to 3 K using a cryostat (see ref. 23 for details). The total efficiency of each memory (used in a double-pass configuration) is 15%. A fibre-optic switch is used to alternate between a 15-ms-long preparation of the two neodymium ensembles as atomic frequency combs on the $^4I_{9/2} \rightarrow {}^4F_{3/2}$ transition, followed by attempts at entanglement creation for another 15 ms. The preparation includes a 4 ms waiting time to avoid fluorescence from atoms left in the excited state. For entanglement creation, continuous-wave light at 532 nm is coupled into a periodically poled (PP) KTP waveguide, leading to the production of pairs of photons at wavelengths of 883 nm and 1,338 nm through SPDC. Photons from each pair are separated on a dichroic mirror (DM) and frequency filtered to below the 120 MHz bandwidth of the quantum memories. Detection of an idler photon at 1,338 nm (using a low-noise superconducting single photon detector[38]) heralds the presence of a signal photon at 883 nm. The signal photon now traverses the switch, a polarizing beamsplitter (PBS) and a Faraday rotator (FR), before a 50/50 beamsplitter (BS) creates single-photon entanglement between spatial modes *A* and *B*. This entanglement is, upon absorption, mapped onto crystals M_A and M_B. After a preprogrammed storage time of 33 ns, the photons are re-emitted and pass through the beamsplitter again. Depending from which output mode of the beamsplitter they emerge, they either reach detector 2 (silicon-based single-photon detector) or are rotated in polarization by the Faraday rotator and reflected by the polarizing beamsplitter towards detector 1.

(concurrence is a measure of entanglement, ranging from 0 for a separable state to 1 for a maximally entangled state). The term V is the interference visibility obtained by recombining optical modes A and B on a 50/50 beamsplitter and is directly proportional to the coherence between the retrieved fields in modes A and B. To obtain a large concurrence, one should maximize V (the coherence) and $p_{10} + p_{01}$ (the probability to detect the heralded photon), and minimize p_{00} and p_{11} (the probabilities of detecting separable states $|0\rangle_A|0\rangle_B$ and $|1\rangle_A|1\rangle_B$ stemming from a lost signal photon and from two signal photons, respectively). To estimate V, p_{00}, p_{10}, p_{01} and p_{11}, we used the set-up of Fig. 1 (see Methods for details). For p_{11}, in particular, we used two different methods, as described in the following.

In the first method, we use a direct measurement of threefold coincidences, that is, involving all three detectors (see Supplementary Information). With a pump power of 16 mW, we obtained $C^{(\mathrm{MLE})} = 6.3 \pm 3.8 \times 10^{-5}$ using a maximum likelihood estimation (MLE) of the threefold coincidence probability, and $C^{(\mathrm{CE})} = 3.9 \pm 3.8 \times 10^{-5}$ using a more conservative estimation (CE). Both estimations yield a concurrence that is greater than 0 by at least one standard deviation, which is consistent with the presence of entanglement between the two crystals. This measurement required 166 h, a period in which two threefold coincidences were observed. The prohibitively long integration time of this method prevented us from attempting it with lower pump powers (that is, for a lower probability of creating more than one pair). Hence, to study how the concurrence changes with pump power, we used a second method based on twofold coincidences, which we now describe.

In the second method, p_{11} is estimated using the fact that our SPDC source produces a state that is very close to a two-mode-squeezed state (TMSS) (see Methods and Supplementary Information). We therefore assume that the measured zero-time cross-correlation $\bar{g}_{s,i}$ is consistent with a TMSS and can be written as $\bar{g}_{s,i} = 1 + 1/p$, where p and p^2 are interpreted as the probabilities of creating one and two photon pairs, respectively (where $p \ll 1$). In practice, $\bar{g}_{s,i}$ is taken as the average value of $g^A_{s,i}$ and $g^B_{s,i}$, where $g^A_{s,i}$ (or $g^B_{s,i}$) is obtained by blocking mode B (or mode A). From the relationship between p and p_{11}, we find

$$p_{11} = \frac{4p_{10}p_{01}}{\bar{g}_{s,i} - 1} \qquad (2)$$

In the Methods and Supplementary Information, we present additional measurements that support our assumption about our source, and show that it leads to a lower bound on the concurrence. We performed a series of measurements for several values of the pump power, which is proportional to p provided $p \ll 1$. Figure 2a shows the interference of the delocalized single photon retrieved from the memories. The visibility does not depend on the pump power, and has an average value of $96.9 \pm 1.5\%$. Figure 2b shows the measured $\bar{g}_{s,i}$, from which it can be seen that reducing the pump power increases the cross-correlation, as expected. Using additional measurements, we estimated the transmission loss, memory efficiency, dark count probability and pair creation probability of our set-up. These values were then used in a theoretical model (shaded region in Fig. 2b) that is in excellent agreement with the measured values of $\bar{g}_{s,i}$, providing additional evidence that the estimated value of p_{11} yields a lower bound on the concurrence (see Supplementary Information). Figure 2c shows the lower bound on the concurrence for all pump powers, calculated using equations (1) and (2). The concurrence decreases with pump power because p_{11} increases, but all other terms in equation (1) depend on photon loss only and hence are approximately constant. Nevertheless, the concurrence remains larger than zero for all used pump powers, consistent with heralded entanglement between the atomic ensembles inside the two crystals. The results of the measurement of the concurrence based on threefold coincidences are plotted in Fig. 2c and agree, within uncertainty, with the results of the method based on measurement of the cross-correlation. The observed values of the concurrence are lower bounds on the amount of entanglement of the detected fields and are almost entirely determined by optical loss. Factoring out the detector inefficiency and interferometer loss yields a lower

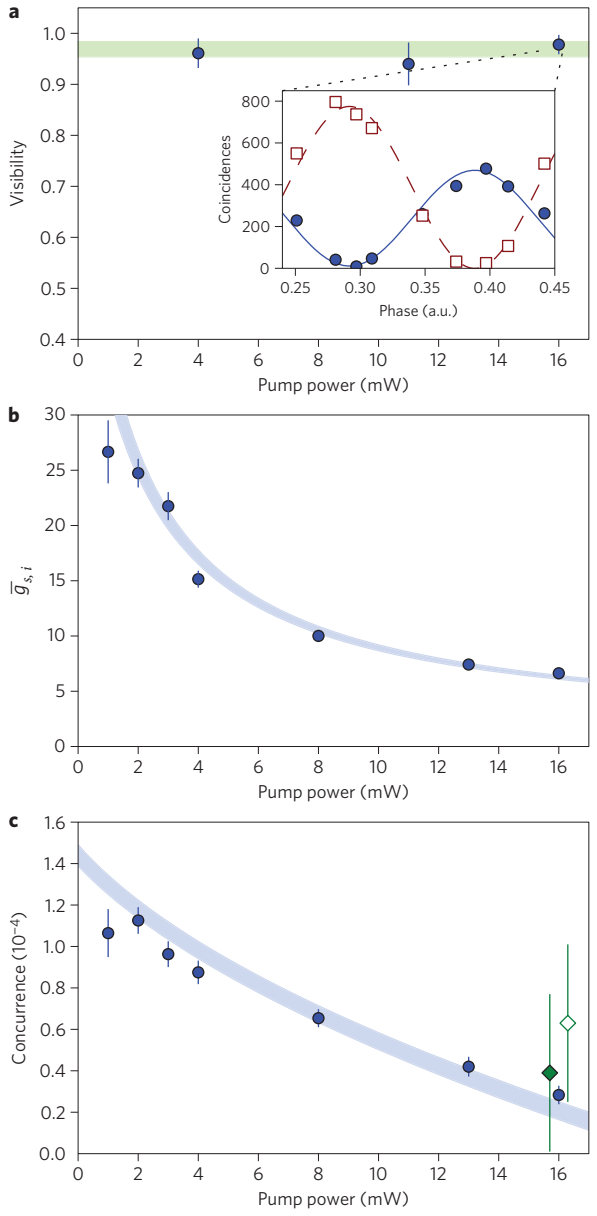

Figure 2 | Results. a, Visibility as a function of pump power. Visibility is approximately constant with an average of 96.5±1.2% (green shaded region). Inset: visibility curves at 16 mW measured with detectors 1 (blue filled circles) and 2 (red open squares) (15 min acquisition time per point; error bars are smaller than the symbols). The different amplitudes result from non-uniform loss after recombination of modes *A* and *B* on the beamsplitter. The visibilities agree, within uncertainty, to the fits. **b**, Zero-time cross-correlation $\bar{g}_{s,i}$ as a function of pump power. The decreasing values agree well with a theoretical model (shaded region; see Supplementary Information). **c**, Lower bound on the concurrence estimated using the cross-correlation measurement as a function of pump power (blue filled circles), calculated using equations (1) and (2), and the mean visibility of **a**. The concurrence decreases with pump power, as expected, but remains positive up to 16 mW. The shaded region corresponds to the model in **b**. All measured values of p_{10}, p_{01} and p_{11} are given in the Supplementary Information. All values are based on raw counts (that is, without subtraction of dark counts and accidental coincidences) and were obtained with coincidence detection windows of 10 ns. Uncertainties are obtained assuming Poissonian detection statistics. The lower bound on the concurrence at 16 mW obtained from measured threefold coincidences using either the MLE (green open diamond) or the CE (green filled diamond) are also shown (horizontally offset for clarity).

bound of ~0.01 for the concurrence of the field retrieved just after the crystals (see Methods).

The high interference visibility indicates that the stored entanglement does not significantly decohere during the 33 ns, and the coherent nature of the storage endures for longer times, as shown previously using storage of weak coherent states[21,28]. Increasing the storage time does, however, lower the cross-correlation function $\bar{g}_{s,i}$, as measured in ref. 23, and this should consequently lower the concurrence of the stored entanglement (this is essentially due to the decrease of the memory efficiency with increasing storage time, as shown in the Supplementary Information and in ref. 23). With Nd^{3+}:Y_2SiO_5 one could, in principle, store entanglement for up to ~1 μs (ref. 21). A promising approach to go beyond these limits, and to allow on-demand retrieval of the stored entanglement, is to implement spin-wave storage[27] to increase the storage times (as demonstrated recently[29] in Pr^{3+}:Y_2SiO_5), and to place the crystal inside an impedance-matched cavity to increase the efficiency[32,33]. Such improvements are necessary for the development of a quantum repeater based on solid-state quantum memories, and are the subject of current research.

In conclusion, we have reported an experimental observation of heralded quantum entanglement between two separate solid-state quantum memories. We emphasize that although the entangled state involves only one excitation, the observed entanglement shows that the stored excitation is coherently delocalized among all the neodymium ions in resonance with the photon, meaning ~1×10^{10} ions in each crystal. Our results demonstrate that RE ensembles, naturally trapped in crystals, have the potential to form compact, stable and coherent quantum network nodes. Moreover, single-photon entanglement is a simple form of entanglement that can be used for teleportation[34] and entanglement swapping operations[3] and can also be purified using linear optical elements[35]. It is also a critical resource in several proposals for quantum repeaters[3,25,36] as it is less sensitive to transmission loss and detector inefficiencies[4]. This, however, is counterbalanced by the extra requirement of phase stabilization over long distances, and the duplication of the resources for post-selecting entanglement shared between two photons, which is needed to implement qubits measurements[4]. Our experimental approach is based on solid-state devices, the key components being the PPKTP chip (the photon source) with an integrated waveguide and the crystal memory. We believe that this approach opens up possibilities for the integration of components, such as frequency filtering directly on the chip[37] or waveguide quantum memories[24]. The prospect of combining solid-state photon sources and quantum memories is therefore attractive for practical future quantum networks. One important challenge in this context is to create entanglement between two remote solids in a heralded way using two distant sources of photon pairs and a central station performing a single-photon Bell state measurement[25], that is, the realization of an elementary link for quantum repeaters.

Methods

Experimental set-up and concurrence estimation. To reveal entanglement in the Fock state basis, one cannot resort to violating a Bell inequality given solely inefficient and noisy single-photon detectors. Instead, quantum state tomography using single-photon detectors was developed[5,13,14]. Implicit to this method are the assumptions that (i) the creation of more than two pairs is negligible and (ii) the off-diagonal elements of ρ with different number of photons vanish (this is valid because no local oscillator providing an aphase reference was used; ref. 5). To estimate V, p_{00}, p_{10} and p_{01}, we used the set-up of Fig. 1 in the following way. First, the visibility V was measured by allowing the re-emitted delocalized photon to interfere with itself using a balanced Michelson interferometer for which the phase was actively stabilized. We then blocked spatial mode *B* to estimate p_{10} by summing the number of detections on detectors 1 and 2, conditioned on a heralding signal. This is justified, as the probability of creating two photon pairs is much smaller than the probability of creating a single one. Probability p_{01} is estimated similarly by blocking mode *A* instead of *B*. Alternatively, we could also estimate the sum $p_{10} + p_{01}$ directly by randomizing the phase of the interferometer, with both arms unblocked (further clarifications and justifications on these measurements are

given in the Supplementary Information). Then, p_{00} is estimated through normalization of the total probability, $p_{00}+p_{10}+p_{01}\approx 1$, which is justified by the fact that $p_{11}\ll p_{10}+p_{01}\ll p_{00}$.

The estimation of p_{11} using the cross-correlation, which is motivated by the results of ref. 13, assumes that all the observed detections stem from a TMSS. In the Supplementary Information, we show that this assumption is conservative and that it yields a lower bound for the concurrence. Using the cross-correlation to estimate p_{11} requires only the measurement of twofold coincidences, rather than threefold coincidences as for the other method. For our specific set-up, this resulted in a reduction of the measurement time by a factor of 10^6 to achieve a similar statistical confidence on the concurrence. Moreover, this method requires no physical modifications to the optical circuit to measure the different components of the retrieved fields, which simplifies its implementation. In the Supplementary Information, we present additional measurement that provide evidence that our source produces a state that is very close to an ideal TMSS, and we summarize the results here. We measured the second-order autocorrelation of the signal (or idler) mode without storage to be $g^{(2)}_{s,s}(0)=1.81(2)$ (or $g^{(2)}_{i,i}(0)=1.86(9)$), which is very close to the maximal value of 2 associated with the thermal photon statistics (the lower observed value can be entirely attributed to the finite temporal resolution of our detectors). We also measured the zero-time second-order autocorrelation function of the heralded signal photon just before storage and obtained $g^{(2)}_{s,s|i}(0)=0.061(4)$ for a pump power of 8 mW, which is consistent with $p\ll 1$.

The observed values of the concurrence are lower bounds on the amount of entanglement of the detected fields and are almost entirely determined by optical loss. To see this, we first note that when both the multi-pair creation probability and the total transmission probability η of the signal photon are small, the concurrence is approximately given by $C\approx\eta(V-2/\sqrt{g_{s,i}-1})$. At 8 mW of pump power, we measured $g_{s,i}\approx 10$, $p_{00}=0.9997831(71)$ and $p_{11}=5.18(40)\times 10^{-9}$, and hence $C\approx 0.3\eta$. With $\eta\approx p_{10}+p_{01}=2.2\times 10^{-4}$, we see that $C\approx 6.6\times 10^{-5}\ll 0.3$. Using this, an estimate of the concurrence of the fields retrieved just after the crystals is obtained by noticing that the transmission η is the product of the probability to find the signal photon inside the fibre per heralding signal (20%), the memory efficiency (15%), the transmission in the interferometer (2.4%) and detector efficiency (30%). Factoring out the detector inefficiency and the interferometer loss yields a lower bound of ~0.01 for the concurrence of the field retrieved just after the crystals.

All results were derived from raw counts, that is, without the subtraction of dark counts and accidental coincidences, and were obtained with coincidence detection windows of 10 ns. We note that there is no measurable temporal overlap between stored and transmitted photons, and that the transmitted photons do not contribute to the entanglement (see Supplementary Information for details, where histograms showing the temporal profiles of detected photons are shown).

Received 24 August 2011; accepted 27 January 2012; published online 4 March 2012

References

1. Kimble, H. J. The quantum internet. *Nature* **453,** 1023–1030 (2008).
2. Briegel, H.-J., Dür, W., Cirac, J. I. & Zoller, P. Quantum repeaters: the role of imperfect local operations in quantum communication. *Phys. Rev. Lett.* **81,** 5932–5935 (1998).
3. Duan, L.-M., Lukin, M. D., Cirac, J. I. & Zoller, P. Long-distance quantum communication with atomic ensembles and linear optics. *Nature* **414,** 413–418 (2001).
4. Sangouard, N., Simon, C., de Riedmatten, H. & Gisin, N. Quantum repeaters based on atomic ensembles and linear optics. *Rev. Mod. Phys.* **83,** 33–80 (2011).
5. Chou, C. W. *et al.* Measurement-induced entanglement for excitation stored in remote atomic ensembles. *Nature* **438,** 828–832 (2005).
6. Gisin, N. & Thew, R. Quantum communication. *Nature Photon.* **1,** 165–171 (2007).
7. Giovannetti, V., Lloyd, S. & Maccone, L. Quantum-enhanced measurements: beating the standard quantum limit. *Science* **306,** 1330–1336 (2004).
8. Nielsen, M. A. & Chuang, I. L. *Quantum Computation and Quantum Information* (Cambridge Univ. Press, 2000).
9. Kok, P. *et al.* Linear optical quantum computing with photonic qubits. *Rev. Mod. Phys.* **79,** 135–174 (2007).
10. Gisin, N., Ribordy, G., Tittel, W. & Zbinden, H. Quantum cryptography. *Rev. Mod. Phys.* **74,** 145–195 (2002).
11. Julsgaard, B., Kozhekin, A. & Polzik, E. S. Experimental long-lived entanglement of two macroscopic objects. *Nature* **413,** 400–403 (2001).
12. Simon, J., Tanji, H., Ghosh, S. & Vuletić, V. Single-photon bus connecting spin-wave quantum memories. *Nature Phys.* **3,** 765–769 (2007).
13. Laurat, J., Choi, K. S., Deng, H., Chou, C. W. & Kimble, H. J. Heralded entanglement between atomic ensembles: preparation, decoherence, and scaling. *Phys. Rev. Lett.* **99,** 180504 (2007).
14. Choi, K. S., Deng, H., Laurat, J. & Kimble, H. J. Mapping photonic entanglement into and out of a quantum memory. *Nature* **452,** 67–71 (2008).
15. Chou, C. W. *et al.* Functional quantum nodes for entanglement distribution over scalable quantum networks. *Science* **316,** 1316–1320 (2007).
16. Yuan, Z.-S. *et al.* Experimental demonstration of a BDCZ quantum repeater node. *Nature* **454,** 1098–1101 (2008).
17. Moehring, D. L. *et al.* Entanglement of single-atom quantum bits at a distance. *Nature* **449,** 68–71 (2007).
18. Tittel, W. *et al.* Photon-echo quantum memory in solid state systems. *Laser Photon. Rev.* **4,** 244–267 (2010).
19. Longdell, J. J., Fraval, E., Sellars, M. J. & Manson, N. B. Stopped light with storage times greater than one second using electromagnetically induced transparency in a solid. *Phys. Rev. Lett.* **95,** 063601 (2005).
20. Hedges, M. P., Longdell, J. J., Li, Y. & Sellars, M. J. Efficient quantum memory for light. *Nature* **465,** 1052–1056 (2010).
21. Usmani, I., Afzelius, M., de Riedmatten, H. & Gisin, N. Mapping multiple photonic qubits into and out of one solid-state atomic ensemble. *Nature Commun.* **1,** 12 (2010).
22. Bonarota, M., Le Gouët, J.-L. & Chanelière, T. Highly multimode storage in a crystal. *New J. Phys.* **13,** 013013 (2011).
23. Clausen, C. *et al.* Quantum storage of photonic entanglement in a crystal. *Nature* **469,** 508–511 (2011).
24. Saglamyurek, E. *et al.* Broadband waveguide quantum memory for entangled photons. *Nature* **469,** 512–515 (2011).
25. Simon, C. *et al.* Quantum repeaters with photon pair sources and multimode memories. *Phys. Rev. Lett.* **98,** 190503 (2007).
26. van Enk, S. J. Single-particle entanglement. *Phys. Rev. A* **72,** 064306 (2005).
27. Afzelius, M., Simon, C., de Riedmatten, H. & Gisin, N. Multimode quantum memory based on atomic frequency combs. *Phys. Rev. A* **79,** 052329 (2009).
28. de Riedmatten, H., Afzelius, M., Staudt, M. U., Simon, C. & Gisin, N. A solid-state light–matter interface at the single-photon level. *Nature* **456,** 773–777 (2008).
29. Afzelius, M. *et al.* Demonstration of atomic frequency comb memory for light with spin-wave storage. *Phys. Rev. Lett.* **104,** 040503 (2010).
30. Sabooni, M. *et al.* Storage and recall of weak coherent optical pulses with an efficiency of 25%. *Phys. Rev. Lett.* **105,** 060501 (2010).
31. Bonarota, M., Ruggiero, J., Le Gouët, J. L. & Chanelière, T. Efficiency optimization for atomic frequency comb storage. *Phys. Rev. A* **81,** 033803 (2010).
32. Afzelius, M. & Simon, C. Impedance-matched cavity quantum memory. *Phys. Rev. A* **82,** 022310 (2010).
33. Moiseev, S. A., Andrianov, S. N. & Gubaidullin, F. F. Efficient multimode quantum memory based on photon echo in an optimal QED cavity. *Phys. Rev. A* **82,** 022311 (2010).
34. Pegg, D. T., Phillips, L. S. & Barnett, S. M. Optical state truncation by projection synthesis. *Phys. Rev. Lett.* **81,** 1604–1606 (1998).
35. Salart, D. *et al.* Purification of single-photon entanglement. *Phys. Rev. Lett.* **104,** 180504 (2010).
36. Sangouard, N. *et al.* Long-distance entanglement distribution with single-photon sources. *Phys. Rev. A* **76,** 050301 (R) (2007).
37. Pomarico, E. *et al.* Waveguide-based OPO source of entangled photon pairs. *New J. Phys.* **11,** 113042 (2009).
38. Verevkin, A. *et al.* Ultrafast superconducting single-photon detectors for near-infrared-wavelength quantum communications. *J. Mod. Opt.* **51,** 1447–1458 (2004).

Acknowledgements

The authors thank H. de Riedmatten, P. Sekatski and J. Laurat for stimulating discussions, and A. Korneev for help with the superconducting detector. This work was supported by the Swiss National Centres of Competence in Research (NCCR) project 'Quantum Science Technology (QSIT)', the Science and Technology Cooperation Program Switzerland–Russia, the European Union FP7 project 247743 'Quantum repeaters for long distance fibre-based quantum communication (QUREP)' and the European Research Council Advanced Grant 'Quantum correlations (QORE)'. F.B. was supported in part by le Fond Québécois de la Recherche sur la Nature et les Technologies.

Author contributions

All authors conceived the experiment. I.U., C.C. and F.B. performed the measurements. I.U., C.C., F.B., N.S. and M.A. analysed the data. All authors contributed to the writing of the manuscript. I.U., C.C. and F.B. contributed equally to this work.

Additional information

The authors declare no competing financial interests. Supplementary information accompanies this paper at www.nature.com/naturephotonics. Reprints and permission information is available online at http://www.nature.com/reprints. Correspondence and requests for materials should be addressed to M.A.